# Control of periodic ferroelastic domains in ferroelectric Pb1-xSrxTiO3 thin films for nano-scaled memory devices

Nesterov, Oleksiy

# Chapter 6

# Nanostructuring ferroelectrics for memory applications.

## 6.1 Summary

In previous chapters we have studied ferroelectric thin films of $PbTiO_3$. The films are interesting due to the highly periodic $a/c-$domains, for which the period is robustly determined by the thickness of the film and the growth conditions (see Chapter 3). We have developed a modification of the theoretical model by Pertsev and Zembilgotov (P&Z model) [1], in order to be able to predict domain periodicity with better accuracy, taking the kinetics of the domain formation into account (see Chapter 3 and 4).

In this chapter, such gained knowledge is used to manufacture ferroelectric nano-structures. We apply the known phenomenon of selective wet etching by polar surfaces [2–4] and use HF acid to preferably etch part of the periodic $a/c-$domain structures in our $PbTiO_3$ films. The aim is to leave only one of the domains untouched while etching the other one. The resulting domain mesh is studied with piezo force microscopy in order to investigate its ferroelectric response. In a first step towards investigating its potential for ferroelectric memory devices, single and multiple bit manipulation is performed.

## 6.2 Introduction

As discussed in Chapter 1, ferroelectric materials are good candidates for active elements in memory devices [5]. In this chapter we use $PbTiO_3$ thin films with domains to test their capabilities as memory elements. These films show periodic $a/c-$domain patterns with $90^o$ domain walls, which are reported to aid domain switching [6]. In addition, $90^o$ walls are also responsible for the enhancement of the piezoelectric response in nano-islands [6]. Reducing the lateral size of the ferroelectric thin film down to the order of the film thickness, decreases clamping of the film to the substrate and allows to measure the piezo-response of such an island [7].

Focused ion-beam [8] and electron-beam lithography [9,10] are the most efficient ways for nano-structuring of oxides. Hard alumina mask during Pulsed Laser Deposition (PLD) has also been used to fabricate standalone $PbZr_{1-x}Ti_xO_3$ nano-capacitors [11]. All mentioned methods have common features: a pattern is fabricated with the help of a mask, which defines the size and period of the nano-objects. Utilizing self-assembling mechanisms that occur spontaneously during the materials deposition is an alternative approach to manufacture nano-objects. The advantage of this method is that it needs less production steps and resources and, importantly, that it can give easier access to sizes below 100 $nm$, which are hard to obtain with the other methods, while maintaining the oxide structural and chemical integrity. High-density ferroelectric memory cells using self-assembled nano-electrodes on a continuous film have previously been reported [12] but the nano-islands had no registry. Indeed, using masks for fabrication has the big advantage of giving rise to ordered arrays of equally spaced nano-structures suitable for memory applications, while the self-assembly approach tends to produce island of diverse sizes and at rather random positions, unless one uses a combined strategy such as block-copolymer templating [13, 14].

In this Chapter in order to overcome this problem, and as an attempt to simplify the process with respect to the use of a template, we intend to use the process of domain formation in ferroelectric/ferroelastic materials, and our control on the domain sizes, in order to fabricate switchable nano-structures. For that we take advantage of the different surface polarity of the different domain variants, defect sites in the crystal lattice (like domain walls) and the preferential etching that they display [2–4]. We use thin $PbTiO_3$ films grown as described in Chapter 3. In these films, as a release mechanism for internal strain, induced by the $DyScO_3$ substrate, highly

periodic and well ordered $a/c-$domains form and their registry is close to that obtained with the help of masks (although more work is needed to optimize this feature).

In addition, the periodicity of such pattern can be as small as 27 $nm$ for our films (see Chapter 3). The periodicity mainly depends on the coherency strain [1] and thus on the mismatch between the substrate and film lattice parameters, and the film thickness. Variation of these parameters allows to vary the $a/c-$domain periodicity and, thus, allows to control the density of nano-structures, which is important for applications: a memory cell with capacity of 1 $Tbit/in^2$ (as the memory roadmap establishes), requires one ferroelectric bit per $25 \times 25$ $nm^2$.

## 6.3 Results

$PbTiO_3$ thin films grown on the top of $SrRuO_3$-buffered (110)-$DyScO_3$ substrates were prepared by PLD. The substrate preparation and growth conditions are described in Chapter 2 and 3 (here we use the fast grown films there described). As described in Chapter 3, such films exhibit very periodic $a/c-$domains structure easily detectable by XRD and AFM measurements. In order to measure the piezoelectric response and to reveal the domain structure, some films were studied with Piezo Force Microscopy (PFM) (see Chapter 1, section 4.3.1 for setup and operating principle).

To proceed with nano-structuring by wet etching, a 120 $nm$ thick $PbTiO_3$ sample was chosen. As seen in Figure 6.1, the $a/c-$domains are highly periodic, especially along one of the two in-plane directions (see Chapter 5 for discussion about the in-plane anisotropy). An average size of a $c-$domain for this sample is $112 \pm 16$ $nm$, which is 80 % of total domain period. We have made samples with much smaller domains size; for example, a 17 $nm$ thick film has only $27 \pm 5$ $nm$ period, which would be better suitable for high density memory applications. However, in order to establish proof-of-concept, a sample with rather large $c-$domains is used to ease the sample treatment and characterization. Before proceeding any further with the sample its ferroelectric structure was investigated with PFM and the results are depicted on Figure 6.1. The amplitude channel shows the $c-$domains as bright areas with a large piezoelectric response; while in between them, the much thinner $a-$domains show no piezoelectric response in the out of plane direction, as expected. The phase channel shows a homogeneous contrast in the $c-$domains indicating that all the

$c-$domains are equally oriented with polarization pointing up.

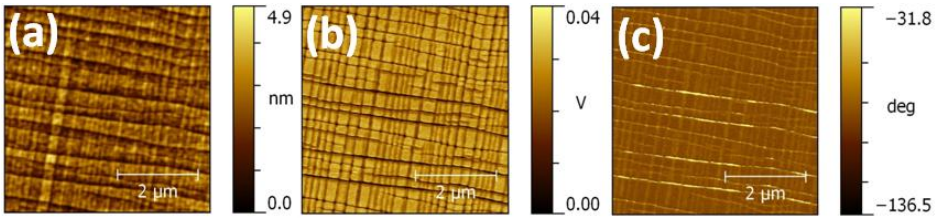


**Figure 6.1:** *PFM images of a 120 nm thick $PbTiO_3$ film. a) topography; b) and c) amplitude and phase channel, respectively, of VPFM.*

Selective etching on ferroelectric $a/c-$domains was performed by buffered 12.5% HF acid. This was done in 3 subsequent steps:

1.1 the sample was submerged into acid for 2 minutes and the beaker containing the acid was placed in ultrasonic bath (Branson 2510) to the aid chemical reaction;

1.2 the reaction was stopped by placing the sample into beakers with di-ionized water. 3 different beakers with water were prepared and the sample was subsequently submerged into each one for 20 seconds in order to make sure there is no acid residue left on the sample;

1.3 an AFM topology measurement was performed in order to check the state of the sample.

All the steps were repeated when necessary. On the Figure 6.2, PFM images are shown of the sample where the selective etching of $\approx 18$ $nm$ of parts of the film is seen. The interpretation of the in-plane piezo-force channels is complicated by the cross-talking with the topography.

In this particular case, the etching process was repeated 9 times until no further height difference was measured, and the etched height was recorded in Figure 6.3, with a resulting 90 $nm$ total height difference. Due to the limited resolution of the technique (tip radius 20-40 $nm$), it is not totally clear if the whole sample thickness (120 $nm$) has been etched. For the last two data points of Figure 6.3 there was no change in height difference observed.

According to the literature, HF should etch faster at positively charged surfaces and at lattice defects [2–4]. In our case, it looks like active etching

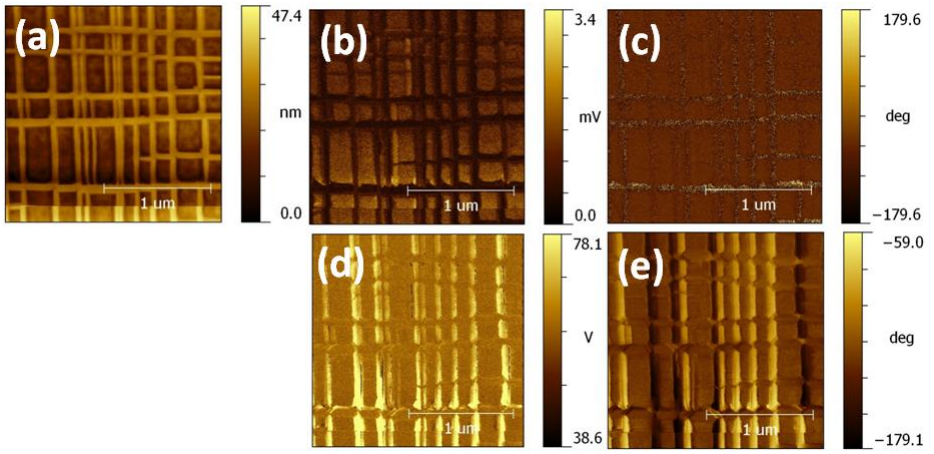


**Figure 6.2:** *PFM images of the same $PbTiO_3$ film of Figure 6.1 after selective etching. The height difference between etched and unetched areas in this image is 18 nm. a) topography; b) and c) out-of-plane piezo-response, amplitude and phase channels respectively; d) and e) in-plane piezo-response, amplitude and phase channels respectively.*

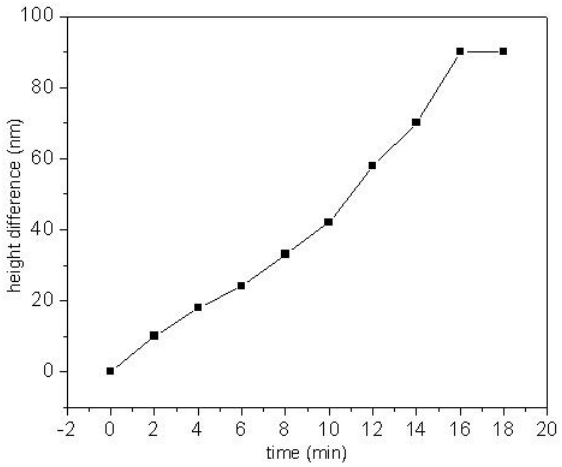


**Figure 6.3:** *Height difference between etched and unetched areas versus etching time, as measured by atomic force microscopy. Average etching rate is 5.5 nm/minute.*

takes part at domain walls. With time, a dip is etched near the domain wall exposing the c-domain side and $a-$domain side (positively charged) to the acid, see Figure 6.4 (a). The etching rate of exposed $a-$ and $c-$domains sides are significantly less than that at the domain wall according to the literature [2–4]. This is supported by TEM measurements in Figure 6.4, where a cross-section TEM image of an HF partially treated sample is depicted. From Figure 6.4 (a) it is clear that the conical shaped material, left after the HF treatment, follows the tilt of a-domains (the domain walls) and that the etching takes place mainly in the $c-$domains. On the other hand, we found a few places where an $a-$domain is etched alongside with the adjacent c-domain, like shown by red dashed lines on Figure 6.4 (b). An explanation for this phenomena will be given later in this chapter.

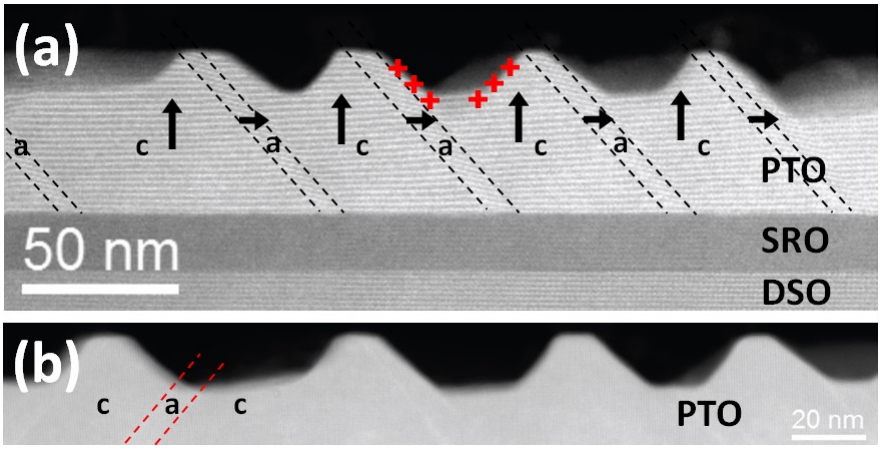


**Figure 6.4:** *Bright field TEM images of a partially etched PTO sample. a) Conical shape of unetched material has its side slopes defined by the tilt of a-domains, marked by black dashed lines; letter "a" and "c", respectively marks a- and c-domains; black arrows depict polarization orientation and red pluses show positively charged exposed a- and c-domain sides. b) Red dashed lines confine an a-domain, which is etched along with adjacent c-domain. Bright field TEM images were taken using a FEI "Titan" microscope by Cesar Magen (INA, Zaragoza, Spain).*

In Figure 6.5 there are topology images of the maximally etched sample, which clearly shows profiles and maximum depth of 90 $nm$. Only when the unetched areas are too close to each other and the tip cannot penetrate, a smaller apparent depth is measured. Once these images are compared

to the images of the untreated sample and TEM images on the Figure 6.4, it becomes clear that the unetched material, although selected by the presence of $a-$domains at the top surface, mainly consists of $c-$domains in the bulk of the film and it is patterned in the in-plane direction by nice and straight domain walls in one direction and wavy walls in the perpendicular direction (see Figure 6.5).

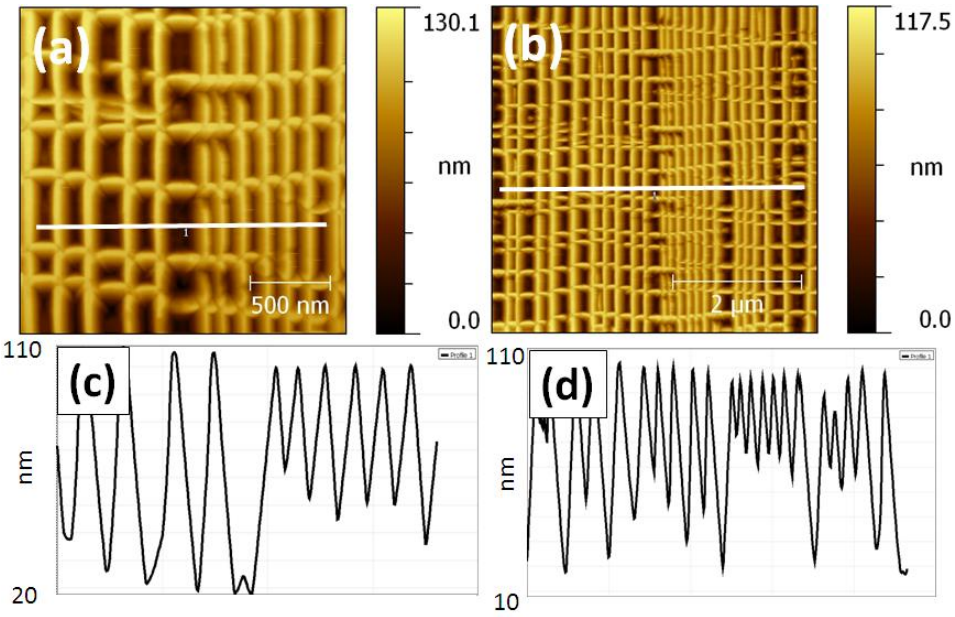


**Figure 6.5:** *AFM topography images of the fully etched sample with crosscuts. a) 2 $\mu m \times 2\ \mu m$ topology image; c) height crosscut along the white line of image (a). The measurements show a 90 nm height difference on the left-side of the image. The size of the tip (≈30-50 nm) prevents measuring the full height on the right-side of the images, where the pattern is denser; the profile line shows a 90 nm height difference; (b) and (d) show similar measurements in a 5 $\mu m \times 5\ \mu m$ area.*

As explained in relation to Figure 6.2 the correlation between the topography and the piezo-response makes it difficult to interpret the PFM images, especially the in-plane response. Thus, in order to study the elec-

trical polarization of the etched sample, it is better to perform PFM measurement at a fixed point in the sample: on the top of an unetched domain the PFM tip was placed, then a DC bias was applied to the tip, and it was slowly cycled from -5 $V$ to +5 $V$. The piezo-response was measured with an AC voltage of 2 $V$ in magnitude at a frequency of 25 $kHz$. The collected data is shown on the Figures 6.6 (a) and (b), as the amplitude and phase channels of the measured response, respectively. These measurements show that coercive voltage for this particular sample-tip system is around 3.8 $V$. Further measurements revealed that the coercive voltage stays within 4 $\pm$ 0.5 $V$ for all tips and different areas used and that it is possible to fully switch down the vector of spontaneous polarization by applying +5 $V$ and more to the tip (same applies in reverse, using negative bias voltage in order to switch the polarization up).

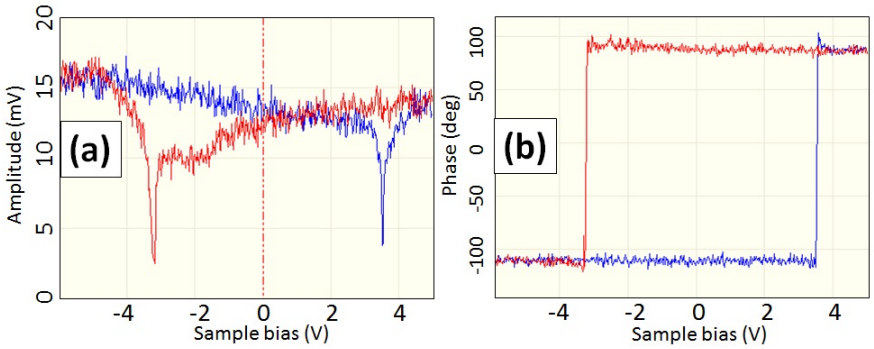


**Figure 6.6:** *PFM hysteresis loops of an unetched part of the sample. a) and b) are, respectively, amplitude and phase signal during a hysteresis cycle. Trace data (voltage ramped from -5 V to +5 V) are in blue and retrace data (voltage ramped +5 V to -5 V) are in red.*

Taking into account the results of the previously described PFM loops, the next natural step is to switch a larger area on the sample surface. This is a simple and efficient way to probe the piezo response of etched, unetched areas and borders between them. Switching is performed by PFM tip scanning over an area of 4 $\mu$m $\times$ 4 $\mu$m with a +7 $V$ DC bias being applied to the tip and with no AC voltage to aid switching. Then the DC voltage is removed and a bigger area of 5 $\mu$m $\times$ 5 $\mu$m is scanned. The AC voltage well below the coercive field is then applied to the tip to probe piezo-response of the sample surface. In order to prove the reliability

of the method, a part of the switched area (2 $\mu$m $\times$ 2 $\mu$m) was switched back to the initial state by applying a negative DC bias to the tip while scanning the area. The results of the switching manipulation are presented on Figure 6.7. Interestingly, it was only possible to switch an unetched part of the sample (bright areas that become dark on the phase channel of Figure 6.7 (c) after switching), while the areas remained under the etched region were not switchable (these areas always stay bright in the phase channel on Figure 6.7(c) before/after the switching). From that, we conclude that, either, the deep areas were completely removed till $SrRuO_3$ bottom layer (which efficiently resists HF) during the acid treatment, or that the remaining $PbTiO_3$ layer is too thin and thus experiences too much clamping for the piezo-response to be measured.

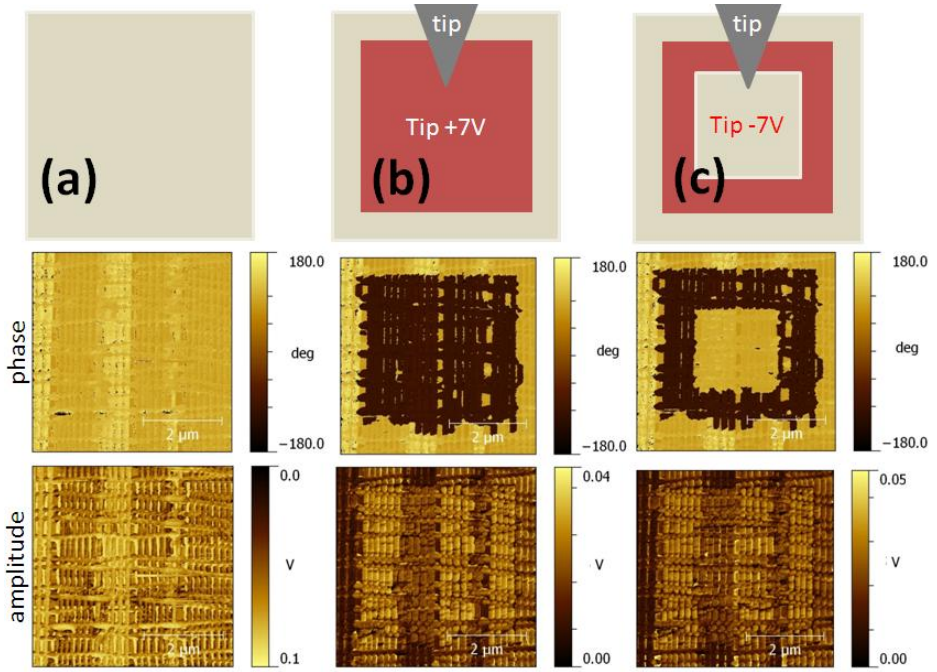


**Figure 6.7:** *Ferroelectric switching inside an area of 5 $\mu$m $\times$ 5 $\mu$m. Rows are sketches (top), phase channel (middle) and amplitude channel (bottom) for different states of the sample: a) images before switching; b) an area of 4 $\mu$m $\times$ 4 $\mu$m switched by applying +7 V DC bias to the tip; c) an area of 2 $\mu$m $\times$ 2 $\mu$m switched back to the initial state by applying -7 V DC bias to the tip.*

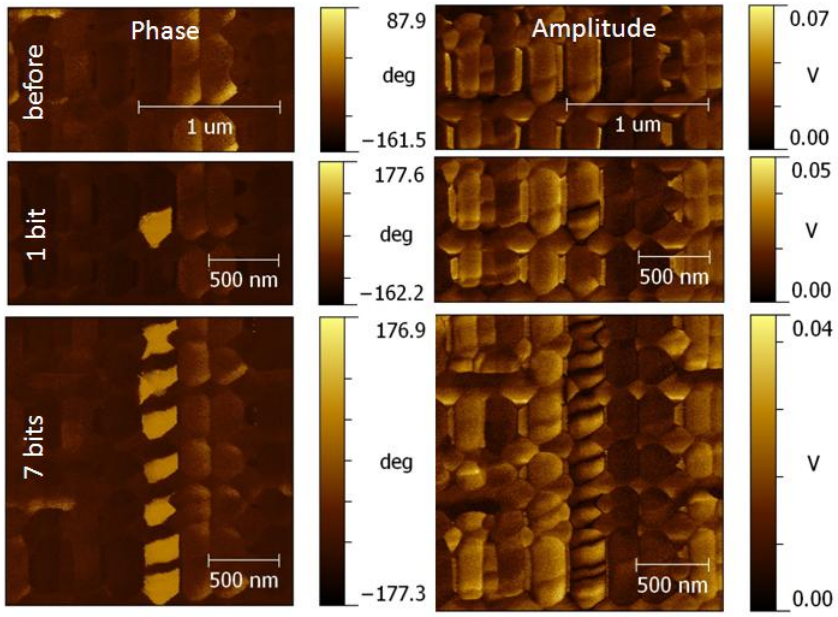


**Figure 6.8:** *Single bits manipulation. Phase (left column) and amplitude (right column) of the out-of-plane piezo-response before switching (top), after switching 1 ferroelectric bit (middle) and after switching 7 ferroelectric bits (bottom).*

Thus it is possible to manipulate the polarization of the unetched parts of the film while the etched regions serve as natural separators between them. In the following then, we will investigate the switching characteristic of the unetched domains in more detail. For this, a PFM tip was placed in the middle of an unetched area of one of the straight domain lines running vertically in the figure (see Figure 6.8). Then a $+7$ $V$ DC pulse was applied to the tip for a duration of one second. A clear contrast in the phase is seen on the "1 bit" phase image in Figure 6.8, indicating that an area of the domain with vertical size of 190 $nm$ has been switched (horizontal dimension is the whole unetched region, of about 180 $nm$). Correspondingly, a dark line appears in the amplitude image, confirming that a domain wall between up and down polarized domains has been created. Then the PFM tip was moved by 200 $nm$ up in the (image) vertical direction and the switching procedure was repeated. In this way 7 points ("bits") were switched. The resulting bits have an average vertical size of $170 \pm 20$ $nm$, while the horizontal size occupies the complete width

of the unetched regions (see "7 bits" image on Figure 6.8).

It can be seen on Figure 6.8 that the shape of the bits is rather unusual: laterally, it is symmetrically confined by the width of the unetched region, as expected. However, in the vertical direction of the image, the switching (always under the same $+7\ V$ DC bias applied for 1 second) appears to be non-symmetric and also confined by, on the one hand, the intersection with the horizontally running domains (what produces a wedge-like shape in the switched bit) and, on the other hand, by what looks like internal boundaries in the material, all parallel to each other and having the same wavy shape across the unetched domains. A close inspection of the amplitude image at the top of Figure 6.8, shows that these features are indeed there and produce some amplitude contrast in the image taken before switching. They are also observed in the other amplitude images of Figure 6.8 also on the unswitched domains. This phenomenon is explained by the presence of extra $a-$domains under the unetched domains, like the one depicted on Figure 6.9, which shows that not all $a-$domains get to the surface, due to the interaction with previously existing domains.

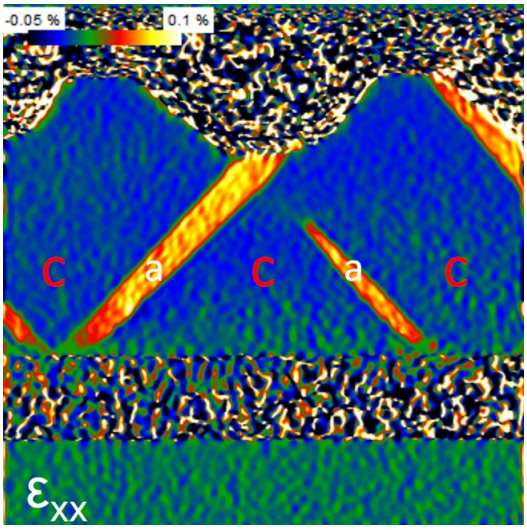


**Figure 6.9:** *Strain map obtained by Geometric Phase Analysis (GPA) of a TEM image of an etched PTO sample. Two a-domains in the center of the image are tilted towards each other and one of them does not get to the surface (so-called "ghost" a-domain). Strain map was prepared using a FEI "Titan" microscope by Cesar Magen (INA, Zaragoza, Spain).*

The switching in the middle of the areas in between two crosses (points where the unetched areas running along perpendicular directions define junctions of four domains, see black circle mark in Figure 6.11 (a)) has also been investigated and the results are presented on Figure 6.10. A $+5$ $V$ DC voltage pulse was applied during 1s to the spots on the sample marked with a red dot on Figure 6.10 (a). These positions are chosen such that each switching center is in the middle of a section in between crosses with different length (each section is bigger than the previous one from top to bottom of the image (the size evolution across the series is marked with white dashed lines on Fig. 6.10 (a)). The resulting phase image on Figure 6.10 (b) shows the switched domains in the middle of the section also being limited by the internal boundaries previously discussed and that there is no clear dependence with the length of the section in between two crosses (see Figure 6.10 (c)).

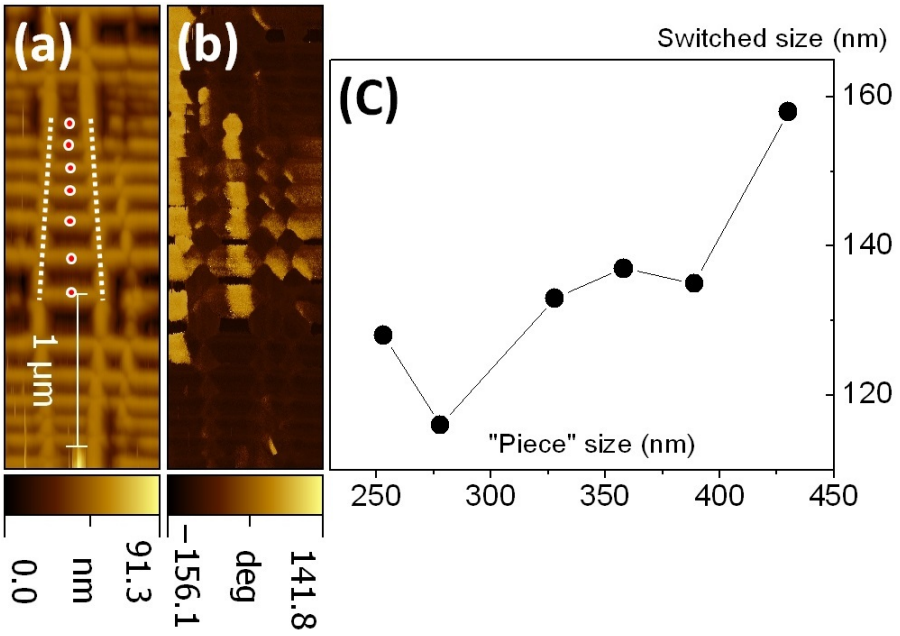


**Figure 6.10:** *Switched domain size versus unetched "piece" size. DC = +5 V, pulse duration is 1 second. a) Topology image, red dots are marks for PFM tip position, white dashed line shows evolution of domain piece size determined by two subsequent "cross" centers; b) phase image. c) resulted plot.*

The same switching procedure described for a single bit (+7 $V$ during 1 second) was applied to the "cross". Each side of a "cross" is switched one after the other. The results are depicted on Figure 6.11. It is known that physically confined objects with spontaneous polarization that experience strict mechanical and electrical boundary conditions can result in unexpected polar configurations [11, 15]. We have not found such unexpected states but, interestingly, we have observed that each side of the cross can be manipulated independently and there is no cross-talking among the four domains (see Figure 6.11 (b) and (c) for horizontal and (d) and (e) for the vertical domains).

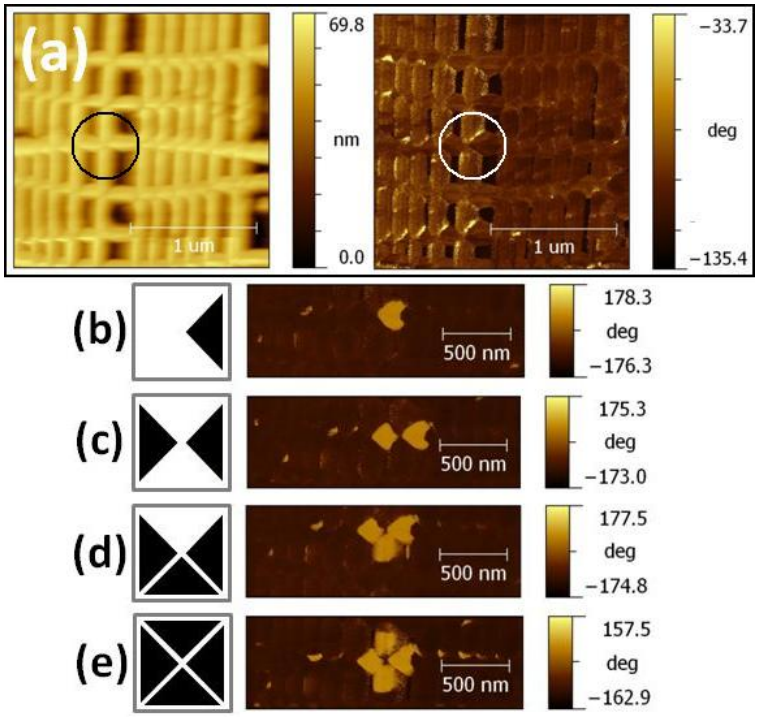


**Figure 6.11:** *"Cross" switching without cross-talking. a) Topology (left) and PFM phase (right) of the sample before switching. Black and white circles mark the "cross" to be switched, respectively. b)-e) Subsequent stages of the switching with sketch on the left, of the area where the tip was placed (in black) and resulting phase image on the right. Bright in the phase image means polarization up and dark means polarization down.*

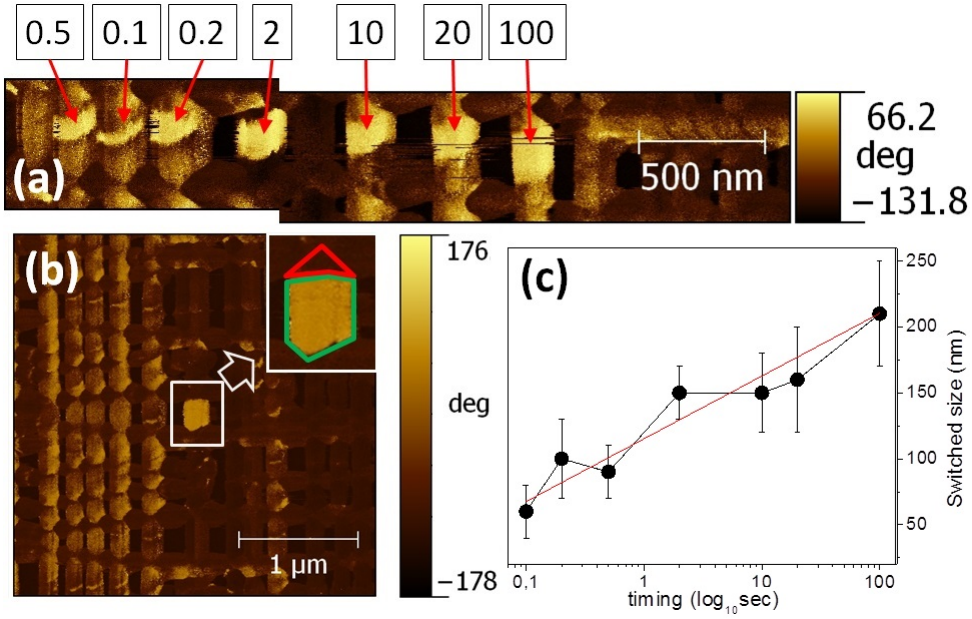


**Figure 6.12:** *Switched domain size versus duration of a DC pulse. a) Phase image of switched domains (+7 V DC, pulse duration marks are on the top in seconds). b) Phase image of a single domain switch at +8 V DC with 300 sec pulse duration with blow-up where green line surrounds the switched part of a domain piece, while red - non-switched part. c) Plot of switched domain size versus DC pulse duration, where red line is a logarithmic fit.*

The DC bias pulse duration is an important parameter which determines the size of the switched bit. In order to investigate this dependence, a PFM tip was used to switch a part in the middle of an unetched areas by applying +7 *V* DC pulse with different durations. Figure 6.12 (a) is a phase image of the switched bits with the pulse duration in seconds marked above the image. A summary of the observed dependency is plotted in Figure 6.12 (c), where it is clear that the switched areas are increased with pulse duration in the short time range from 0.1 to 2 seconds and then become less dependent on time. This type of logarithmic behavior is also found in literature [16, 17]. It can be seen that the switched area increases with pulse duration, but it never fills the whole section in between two domains junctions or crosses, again limited by the internal "ghost" domain boundaries discussed earlier. In order to check the robustness of

such boundaries, a +8 $V$ DC pulse was applied during 300 seconds. The resulting phase image of the switched area is in Figure 6.12 (b). Even with such strong electrical driving force it was not possible to switch the whole section between two crosses (see red line surrounding the non-switched bit on blow-up on Fig. 6.12 (b)), while the rest of the unetched domain were switched (see green line on blow-up on Fig. 6.12 (b)).

These results show that there is the opportunity to use these samples as memory devices, where the memory bits are naturally separated, cross-talking of close-by bits is avoided and the writing conditions are not critical. The size of each bit is defined by width of the unetched areas, which depends on the original domain width and the etching time (this is about 200-300 $nm$ in the present example but it can be made smaller, even down to 30 $nm$) in one direction. In the vertical direction the size is limited by internal boundaries (most possibly ghost a-domains, as discussed above).

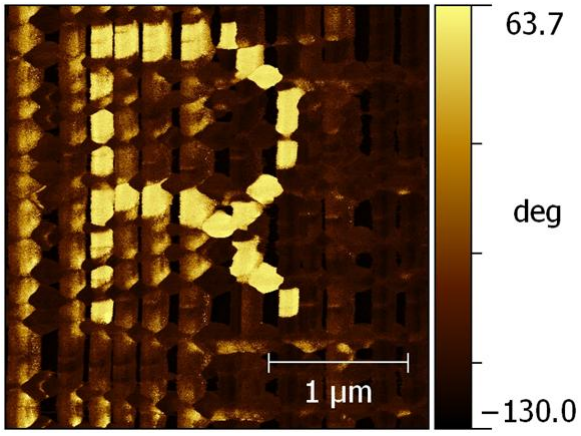


**Figure 6.13:** *PFM manual manipulation with the sample surface. The letter 'R' has been written bit by bit.*

To visualize sample performance as a memory device, switching of bit patterns were performed. Two approaches were used: manual and automated writing (performing switching according to a pre-determined pattern). Manual patterning was done by placing the PFM tip manually to each position on the sample. A resulted phase PFM image is on Figure 6.13. A clear 'R' letter can be seen on it, which consists of single bits. The bits were switched separately one by one. Accuracy in the tip position is an advantage of this method but, on the other hand, it is very time

consuming. The tool "NanoMan" in the NanoScope software package by Veeco (now Bruker) was used for automated manipulation. On the Figure 6.14 (a) there is a phase image of the sample before patterning. An image was fed to the software, see Figure 6.14 (b). As a result, the software moves the PFM tip across the sample accordingly applying the required voltage. The phase image recorded after manipulation is on Figure 6.14 (c). This method allows for fast and efficient patterning but it is not possible to position PFM tip accurately on the desired place of the sample.

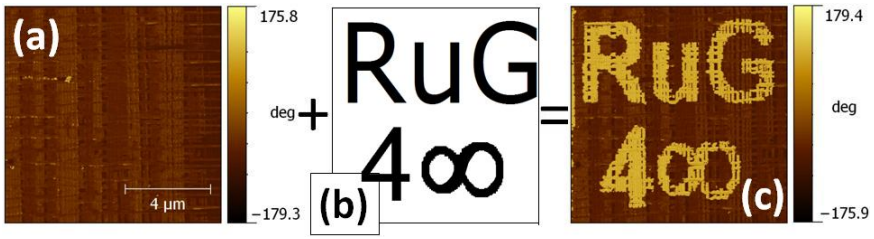


**Figure 6.14:** *Automated manipulation of ferroelectric bits by PFM software. The text "RuG for Infinity" (the motto of the 400 anniversary of the University of Groningen, celebrated this year) has been designed and provided to the software (b). The PFM tip with a bias voltage applied to it follows the image automatically and reproduces it on the ferroelectric sample (a) sample before- and c) after- automated bits writing).*

## 6.4 Conclusion

We have used the ferroelastic/ferroelectric domain patterns investigated in previous chapters to obtain a highly periodic selective etching and thus nano-structuration of a 120 *nm* thick $PbTiO_3$ film. The treated sample has its average vector of spontaneous polarization pointing out of the plane of the sample. This feature allows to switch a single bit by applying field normal to the sample surface. Apart from other factors like the magnitude of the applied voltage or its duration, the size of a single bit is mainly and robustly determined by the width of the unetched regions and the original domain width, which are in turn, controlled by the film thickness and growth conditions (see Chapter 3). Writing an area on the sample according to the pattern shows the possibility to automate the switching process, which is crucial for the next step in a memory development.

# Bibliography


[1] N.A. Pertsev and A.G. Zembilgotov, J. Appl. Phys. **78**, 6170 (1995).

[2] S. Grilli, P. Ferraro, P. De Natale, B. Tiribilli and M. Vassalli, Appl. Phys. Let., **87**, 233106 (2005)

[3] I. E. Barry, G. W. Rossa, P.G.R Smith, R. W. Eason, G. Cook, Materials Letters **37**, pp. 246-254 (1998)

[4] G.L. Pearson, W.L. Feldmann, J. Phys. Chem. Solids, **9**, pp. 28-30 (1958)

[5] O. Auciello, J. F. Scott and R. Ramesh, Physics Today, 51, **7**, 22 (1998)

[6] V. Nagarajan, A. Roytburd, A. Stanishevsky, S. Prasertchoung, T. Zhao, L. Chen, J. Melngailis, O. Auciello and R. Ramesh, Nature Materials **2**, 43 - 47 (2003)

[7] K. Lefki and G. J. M. Dormans, J. Appl. Phys. **76**, 1764 (1994)

[8] J. Melngailis, J. Vac. Sci. Technol. B **5**, 469-495 (1987)

[9] V. R. Manfrinato, L. Zhang, D. Su, H. Duan, R. G. Hobbs, E. A. Stach and K. K. Berggren, Nano Lett., 13 **4**, pp. 1555-1558 (2013).

[10] M. Alexe, C. Harnagea, A. Visinoiu, A. Pignolet, D. Hesse, U. Gsele, Scripta Materialia, **44**, pp. 1175-1179, 18 May (2001)

[11] B. J. Rodriguez et al., Nano Lett. **9**, 1127 (2009)

[12] M. Alexe, J. F. Scott, C. Curran, N. D. Zakharov, D. Hesse and A. Pignolet, Appl. Phys. Lett. **73**, 1592 (1998)

[13] N. M. Aimon, H. K. Choi, X. Y. Sun, D. H. Kim and C. A. Ross, Adv. Mater. (2014)

[14] J. Varghese, R. W. Whatmore and J. D. Holmes, J. Mater. Chem. C, **1**, 26182638 (2013)

[15] A. Gruverman et al., J. Phys. Cond. Matter **20**, 342201 (2008)

[16] T. Tybell, P. Paruch, T. Giamarchi and J.-M. Triscone, Phys. Rev. Lett. **89**, 097601 (2002)

[17] A. Gruverman, B. J. Rodriguez, C. Dehoff, J. D. Waldrep, A. I. Kingon and R. J. Nemanich, Appl. Phys. Lett. **87**, 082902 (2005)